Sample-efficient Search for Satisfactory OLED Designs

Khashayar Mohammadi[1], Michael McCourt[2]*, Paul Leu[1]

[1]Laboratory for Advanced Materials at Pittsburgh
University of Pittsburgh
pleu@pitt.edu, khashayar@pitt.edu
[2]SigOpt, an Intel company
mccourt@sigopt.com

Abstract

Higher efficiency OLEDs can operate with less power, but identifying efficient designs can be a slow process because the cost of fabricating proposed designs is extreme. Computational simulations are more expedient, but they provide only an approximation to the eventual manufactured outcome. Moreover, blind search for the optimal structure with simulations is not a favorable choice due to the number of design parameters and high computational costs. We apply the Constraint Active Search methodology to identify a diverse set of designs which all have suitably high efficiency for eventual consideration for physical fabrication.

Introduction

Organic light emitting diodes (OLEDs) are a fundamental part of modern electronics; cell phones, monitors and television screens use OLEDs as a power-efficient mechanism for facilitating their displays. An OLED device is made of multiple layers to emit the light. The most generic OLED device is made of a cathode layer, an organic layer which the light is generated in, a transparent anode layer and a glass substrate. Although the modern manufactured OLEDs are much more complicated and have many different layers and multiple doped organic layers to increase the internal quantum efficiency, we consider a less complex model to simulate for the sake of simplicity and because most of the additional layers, mainly organic layers, have very close refractive index and this does not affect the out-coupling efficiency that we are investigating. See Figure 1 for a depiction of the OLEDs we consider here.

In the presented model, to increase the extraction efficiency, an anti-reflection layer is introduced between the Anode (ITO) and the glass substrate. In general, a middle layer can be used to reduce the reflection of light at the contact surface of two materials with different refractive indexes. The additional layer gives the best performance if its refractive index follows this equation: $n_3 = \sqrt{n_1 \cdot n_2}$. Refractive indexes of the ITO and glass are 1.94 and 1.46 respectively at the wavelength of 520nm (green light) which the simulations are performed at. The best material to use as anti-reflection

---

layer should have refractive index of $n = \sqrt{1.94 \cdot 1.46} = 1.68$.
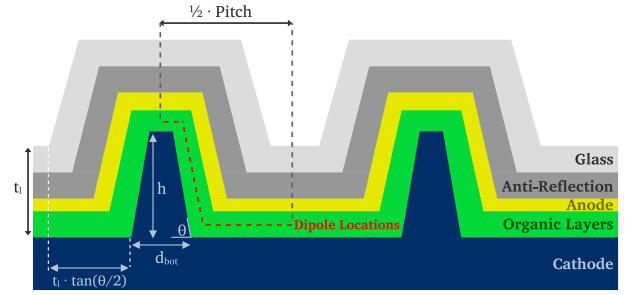

Figure 1: This graphic representation of the cross-section of an OLED showing the elements of OLED design under consideration during our experimentation. Text in red denotes parameters we consider tuning, and text in black denotes design choices we have fixed for this article.

Efficiency of an OLED device is represented by External Quantum Efficiency (EQE) which encompasses two distinct factors: internal quantum efficiency and out-coupling efficiency. EQE is the ratio of the number of the emitted photons to the number of the injected electron charges (Glowacki et al. 2012). Equation 1 defines the OLED efficiency:

$$\text{EQE} = \gamma \cdot \eta_{\text{rad, eff}} \cdot \eta_{\text{S/T}} \cdot \eta_{\text{out}} \qquad (1)$$

in which $\eta_{\text{int}} = \gamma \cdot \eta_{\text{rad, eff}} \cdot \eta_{\text{S/T}}$ is defined as internal quantum efficiency and η_{out} is the out-coupling efficiency. Internal quantum efficiency encircles efficiencies pertaining to the used materials and manufacturing quality such as electrical efficiency (γ), effectiveness of the emitter ($\eta_{\text{rad, eff}}$), and the portion of excitons turning into emitted photons ($\eta_{\text{S/T}}$), while the out-coupling efficiency (η_{out}) represents the efficiency of the optical environment design.

During the last two decades, many successful works have been done to increase the internal quantum efficiency to 100% (Adachi et al. 2001; Xiao et al. 2009; Zhang et al. 2015; Williams et al. 2007) and today's problem with low efficiencies of OLED devices is mainly the out-coupling efficiency and the trapped light within the OLED structure that keeps the EQE low. Department of Energy has set the target extraction efficiency for OLED devices to 75% for

2035 and 60% for interim 2025 target (Pattison et al. 2020). Finite-difference time-domain (FDTD) simulations helps us to understand the out-coupling efficiency of different OLED structures and enables us to search for optimal designs. To perform FDTD simulations, Lumerical software has been used.

Many different OLED structures were simulated and manufactured to increase the extraction efficiencies. Microlens arrays was casted on top of the glass substrate by (Wei and Su 2004; Ho et al. 2013) and showd upto 56% and 74% improvement in luminance efficiency respectively. Also, OLED devices with cylindrical microlens arrays was manufactured by (Lee et al. 2008) but comprised the image quality to increase the outcoupling efficiency. A corrugated oled model was proposed and manufactured by (Schwab et al. 2014) and their measurements showed 13.5% increase in EQE. In their model corrugation are in the all OLED layers similar to the conformal structure proposed in this article.

In this article, we focus on improving the OLED extraction efficiency (out-coupling efficiency) through a conformal OLED structure. Previous research has shown that tempering with flat structures can be a promising method to achieve higher light extraction values or lower reflections. see (Haghanifar et al. 2020) for an application of aditively manufactured cones on top of the glass to reduce the reflection of a piece of glass.

Numerical Simulation

Lumerical FDTD is a numerical solver of Maxwell's equations for complex geometries and is usable for all electromagnetics and photonics problems. For more information please see (Lumerical Inc. 2021a).

The simulated model is composed of the cathode layer: Aluminum, organic layer(s): $Ir(ppy)_3$, Anode: ITO, anti-reflection layer: Al_2O_3, and glass substrate. In practice, emission occurs at all points in the organic layer; though, to be able to model the emission of light in simulations we should consider enough number of dipoles within the organic layer to cover the whole area properly and average the results over all dipoles to obtain the final result. The vertical location of the dipoles within the organic layer is assumed to be at half of the layer thickness (the red dashed line in Figure Figure 1). Also due to the symmetry, we only consider half of the device pitch to place the dipoles.

FDTD is inherently a coherent simulation method. To achieve incoherent results which we are interested in, we should understand and consider coherence in FDTD simulations. For comprehensive explanation please see (Lumerical Inc. 2021b). For our 2D OLED simulations, we should consider spatial incoherence meaning to avoid including more than one dipole in each simulation and also avoid periodic boundary conditions when electromagnetic filed is not close to zero at boundaries, and also consider polarization incoherence meaning to average the results over three orthogonal dipoles at each dipole location to obtain the results for an unpolarized beam. Simulation domain or width of the OLED device should be large enough to get an accurate result. Photons traveling between the OLED layers can

eventually find their way out of the structure after travelling through a couple of conformal structures. Therefore, it is necessary to make sure the simulation width has been chosen large enough.

Thickness of the layers in the simulated OLED devices in this paper are shown in Table 1. Although for further optimization, layer thicknesses can be chosen as optimization variables, in all simulations in the current study these parameters are fixed and are not included for optimization.

Also note that the initially defined pitch value will be modified during the simulation according to the layer thicknesses by the factor of $2 \cdot t_1 \cdot \tan(\theta/2)$ to ensure each layer has the same thickness around the cones and also each cone has properly spaced by their adjacent structures. See Figure 1 for details.

Table 1: Thickness of OLED layers for the simulated device.

Layer	Thickness
Organic Layer(s)	200 nm
Anode	100 nm
Anti-reflection	200 nm
Glass	200 nm

To ensure that performed FDTD simulations are valid and accurate, three certain parameters that directly affects the computational accuracy was investigated: **mesh size**, **simulation width**, and **number of dipoles**.

Mesh size. FDTD method solves Maxwell's equations by discretization of the simulation domain and time. Similar to the all other discretized computational methods, usually, smaller mesh size means higher accuracy but also means higher computational times. To find the best uniform mesh size, multiple simulations with different mesh size for two different structures, one with smaller geometries and one with larger geometries, was performed. Table 2 shows the structures used in convergence tests.

Table 2: Size of the structures investigated for convergence tests.

Structure	Height	Pitch	D_{bot}	D_{top}
Small	800 nm	400 nm	300 nm	100 nm
Large	700 nm	2500 nm	2000 nm	500 nm

Figure 2 shows that by choosing mesh size smaller than or equal to 10nm, we can have reliable results for OLED extraction efficiency values. For faster but a slightly inaccurate results 10nm mesh size is favorable to use. To have high accuracy 5nm mesh size should be used in the simulations.

Simulation width. As discussed before, the simulation domain should be chosen large enough so that we make sure the obtained extraction efficiency has converged properly to the actual value. If a small simulation domain is selected then the result value for the extraction efficiency would be lower. shows how extraction efficiency changes for different initial simulation domains.
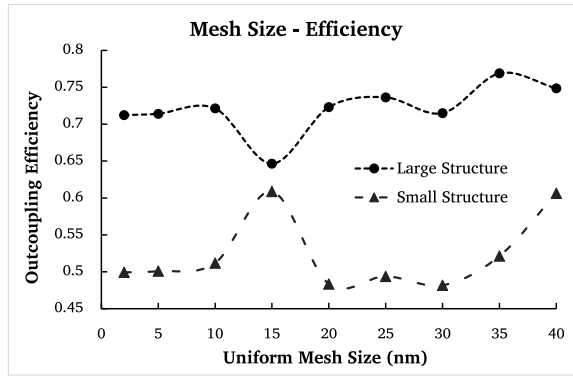
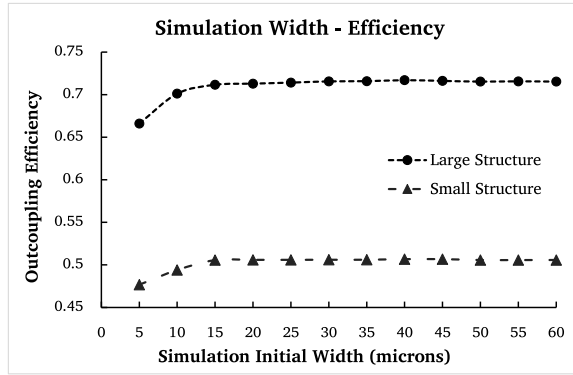Figure 2: Convergence test for uniform mesh sizes.

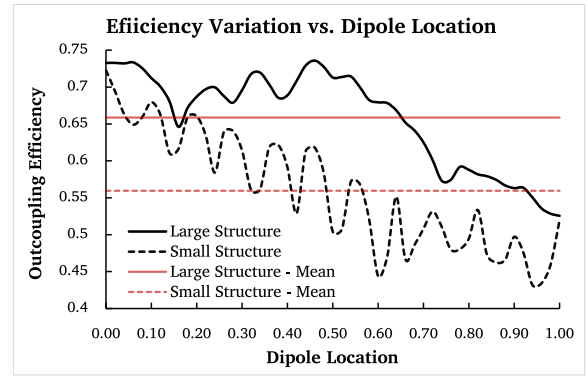Figure 3: Convergence test for different simulation domains.

Figure 4: Variation of the out-coupling efficiency for different dipole locations.
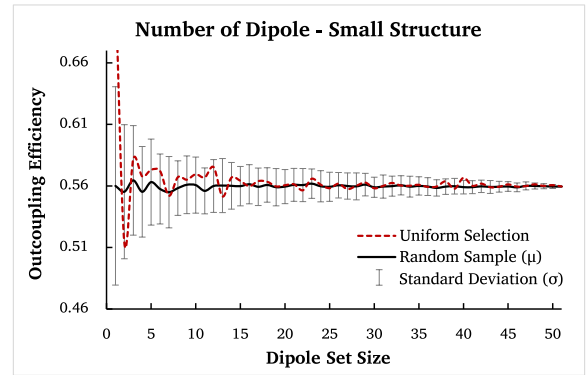
Figure 5: Comparison of the uniform and random dipole selection approaches for the small structure.

Number of dipoles. One important parameter in the OLED simulations is the number of dipoles. The red dashed line in Figure 1 shows all the possible locations for the dipoles. To have the most accurate result, unlimited number of dipoles should be averaged on this line, but it is obviously impossible. To have an insight of how efficiency changes for different dipole locations, Figure 4 shows the variation of the out-coupling efficiency for 50 uniformly distributed dipoles along half the pitch for each of the two structures. Red lines denotes the average values of these 50 dipoles which we can safely consider as the actual out-coupling efficiency of the OLED device.

Before delving into the proposed optimization procedure in this paper, we represent two simple approaches for dipole selection to show their difference and accuracy: **uniform selection** and **random selection**.

For uniform selection, we can consider selecting e.g. 10 dipoles uniformly distributed in half the pitch (red dashed line in Figure 1) and average efficiencies over those 10 dipoles. For random selection, we can randomly choose e.g. 10 dipoles and average the results. Figure 5 and Figure 6 show the results for these two approaches. In random selection approach, for each sample size (e.g. 10 randomly selected dipoles) the sampling was repeated 100 times and the mean and standard deviation of the extraction efficiencies of these 100 samples were calculated and plotted.

Our goal in this research is to maximize the OLED extrac-

tion efficiency, denoted η_{out}, as measured as the fraction of the emitted photons form the OLED through the glass substrate.

Identifying Satisfactory Designs

As indicated earlier, we only consider the implications of the additive manufacturing on the efficiency – the other OLED elements are fixed throughout our experimentation. Our search domain (see Figure 1 for reference) is defined as

- Simulation Domain: $a \in [100, 2000]$ nm
- Cone Top: $d_{\text{top}} \in [100, 2000]$ nm
- Cone Bottom: $d_{\text{bot}} \in [100, 2000]$ nm
- Height: $h \in [100, 2000]$ nm

To enforce the cone shape during manufacturing we enforce the domain constraints:

- Simulation Domain > Cone Bottom, and
- Cone Bottom > Cone Top.

We denote this constrained search space as $\mathcal{X}$ and each individual design as $\mathbf{x} \in \mathcal{X}$.

As described earlier, our goal in this project is to identify an OLED design involving these 4 parameters which can surpass 75% extraction efficiency. We use the numerical simulation strategy described earlier to search for this
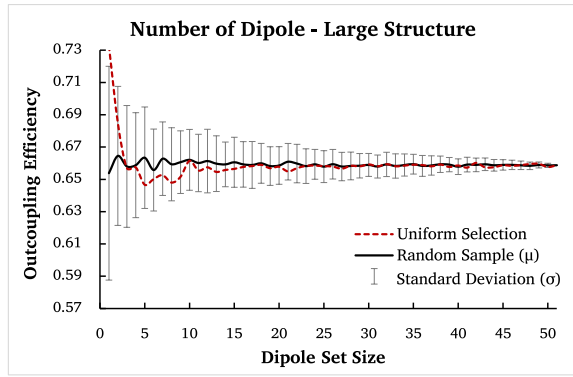
Figure 6: Comparison of the uniform and random dipole selection approaches for the large structure.

design, but the numerical simulation is only an approximation to the performance of the ultimate fabrication. The mesh size, simulation width and number of dipoles involved in the simulation all affect the accuracy; additionally. Furthermore, as discussed in (Haghanifar et al. 2020), the physical manufacturing process incurs its own imprecisions in actually producing the prescribed design (the maskless reactive ion etching fabrication process (Haghanifar et al. 2017) will not be precise at 1 nm length scales).

Constraint Active Search

To account for the gap between the problem we are studying (the efficiency estimated in our numerical simulation) and the actual problem we want to study (the efficiency of the physical OLED), we utilize Constraint Active Search (Malkomes et al. 2021). This strategy replaces the optimization of efficiency with a search for a diverse set of designs satisfactory efficiency; the final choice, or choices, of fabrication can be made from this set based on other criteria (such as fabrication speed, consistency, durability, etc). We choose 70% as our satisfactory value, under the belief that the gap between simulation and fabricated performance may be 5%.

Constraint active search (CAS) requires an acquisition function, and we use the probability of success acquisition function

$$g(\mathbf{x}) = P(Y_{\mathbf{x}} > \tau | \mathcal{D}), \qquad (2)$$

where $Y_{\mathbf{x}} | \mathcal{D}$ denotes a Gaussian process (Fasshauer and McCourt 2015) Y considered at the location $\mathbf{x}$ conditioned on $\mathcal{D}$, the data observed thus far ($\mathbf{x}_i$ and $\text{EQE}(\mathbf{x}_i)$ values) and τ represents our definition of success (which we stated will be 70%).

In (Malkomes et al. 2021), the authors use a resolution parameter to define a desire to search away from previously observed $\mathbf{x}$ values – in this setting, this has the effect of accounting for our limited manufacturing precision by not over-resolving a small region of the design space. We use a resolution parameter of 150 here, which is incorporated into our acquisition function optimization process by only optimizing over points which are at least 150 nm away in design

space, i.e., the next design to test satisfies

$$\max_{\mathbf{x} \in \mathcal{X}} g(\mathbf{x}), \text{ such that } \forall \mathbf{x}_i \in \mathcal{D}, \|\mathbf{x} - \mathbf{x}_i\|_2 > 150.$$

In the random search (RS) settings, we also account for the limited manufacturing precision by restricting all parameters to 10 nm increments, i.e., Cone Bottom can only take values $100, 110, 120, \ldots, 2000$ nm; this matches the strategy used in (Haghanifar et al. 2020).

Search Implementation Considerations

For each design $\mathbf{x} \in \mathcal{X}$, the resulting efficiency evaluation $\text{EQE}(\mathbf{x})$ is the sum of three integrals: the x, y and z-axis emissions integrated over the possible dipole locations as depicted with the dashed red line in Figure 1. Without loss of generality, the dipole locations can be parametrized as being within a domain $[0, 1]$, thus the efficiency values may be written as

$$\text{EQE}(\mathbf{x}) = \int_0^1 \text{EQE}_x(\mathbf{x}; p) \, \mathrm{d}p$$
$$+ \int_0^1 \text{EQE}_y(\mathbf{x}; p) \, \mathrm{d}p$$
$$+ \int_0^1 \text{EQE}_z(\mathbf{x}; p) \, \mathrm{d}p,$$

where $\text{EQE}_x(\mathbf{x}; p)$, $\text{EQE}_y(\mathbf{x}; p)$ and $\text{EQE}_z(\mathbf{x}; p)$ are the efficiencies along the x, y and z axes for a single dipole $p \in [0, 1]$.

These integrals can be computed in any fashion, but we can leverage the structure of our optimization algorithm to estimate the integrals at low accuracy before improving the quality of only those with high efficiency. We estimate the integral with Quasi Monte Carlo (Choi et al. 2020+), allowing up to 33 total points in the estimate; for example, in the x-axis, this would look like:

$$\int_0^1 \text{EQE}_x(\mathbf{x}; p) \, \mathrm{d}p \approx \frac{1}{n} \sum_{i=1}^{n} \text{EQE}_x(\mathbf{x}; p_i) \qquad (3)$$

where p_i come from the Halton sequence and $n \leq 33$.

After a new design $\mathbf{x}$ has been chosen (whether through RS or CAS) We use the first 5 p_i in the sequence and study the mean and variance of the integral estimator in (3). As the optimization/search progresses, if the integral for a given design $\mathbf{x}$ has *too much variance*, another more dipoles are included in the integral estimate (which reduces the variance), up to 33 total dipoles. This strategy is analogous to that of early stopping in machine learning (Caruana, Lawrence, and Giles 2001) – it has also been used in a medical imaging setting (McCourt, Dewancker, and Ganci 2016).

In RS, we consider a design to have too much variance if its 2 standard deviation confidence interval contains the mean of the design with the highest mean seen thus far (including the highest mean seen thus far). For CAS, a design has too much variance if its 2 standard deviation confidence interval contains the efficiency threshold 70%. To seed the optimization/search, we initialize with 12 designs drawn randomly from $\mathcal{X}$ before conducting any termination.
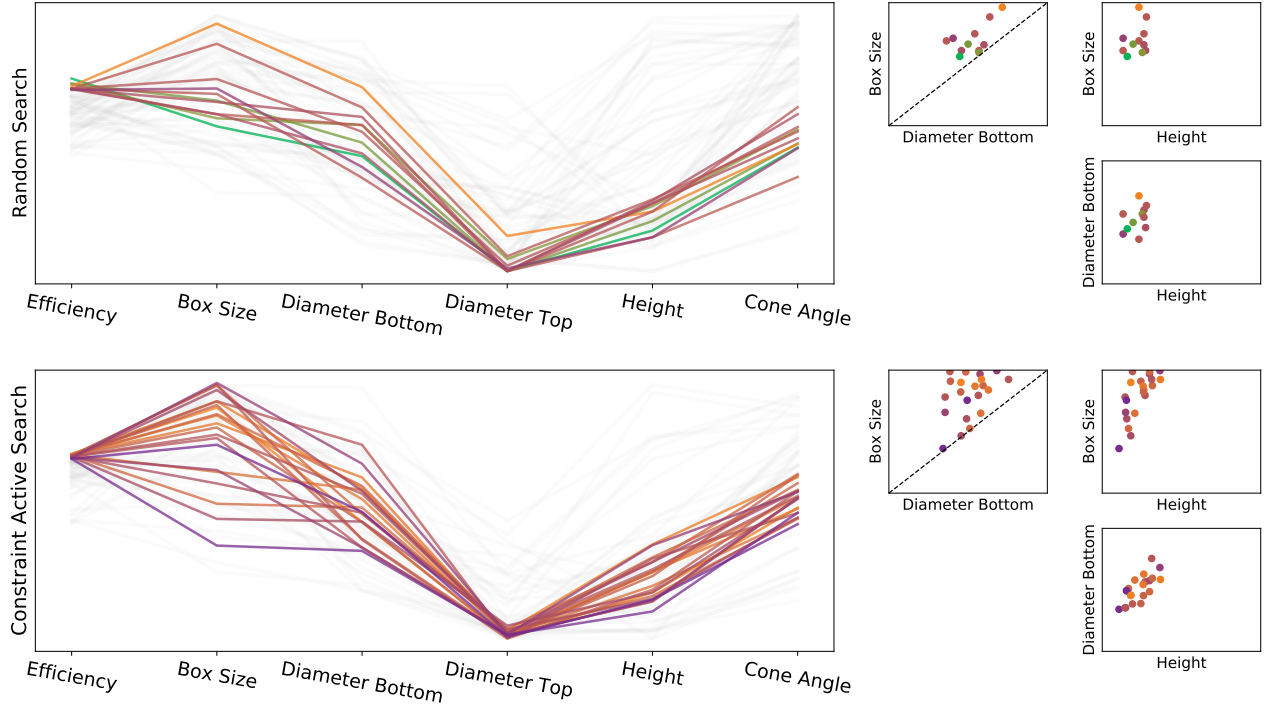
Figure 7: The top row of results is for RS and the bottom row is for CAS. The parallel axes plots and the scatter plots show that CAS more completely explores the satisfactory region but without concern for highest performance. Only the points with mean efficiency above 70% are shown in color. The Cone Angle is a additional characteristic of the manufactured shape: the angle of the cone rising off the base surface (plotted with limits $[0, \pi/2]$). The dashed black line in the scatter plots is a physical constraint place on the parameters.

To balance between decreasing variance and searching $\mathcal{X}$, we keep a global max dipole count, starting at 5 and increasing by 4 (up to 33) each time a new $\mathbf{x}$ is considered. After the new $\mathbf{x}$ has computed its dipoles up to the global max (allowing for early termination), all the previously considered designs are also given the next 4 dipoles in the Halton sequence if their efficiency estimator is considered to have too much variance.

For CAS, we use the Gaussian process estimates of mean and variance, and for RS we use the standard Monte Carlo estimate. After each new dipole is computed, we refit the Gaussian process hyperparameters using maximum likelihood estimation. The covariance kernel for the Gaussian processes is the C^4 Matérn kernel, and we use a constant polynomial mean fit with generalized least squares.

Experimental Results

In our experiment, we gave both RS and CAS 500 dipoles worth of computations to consider and studied the resulting designs. Table 3 shows that CAS was able to produce 10 extra satisfactory designs despite only creating roughly the same number of unique designs. This is partly possible through more intelligently choosing the sampling locations, and also because the Gaussian process model used in CAS provides more accurate estimates of the fully accurate integrals in (3) (though the covariance incorporating data from other designs in the efficiency estimates).

Strategy	# Designs	# Satis. Designs	Avg. # Dipoles per Unsatis.
RS	67	11	6.875
CAS	68	21	5.071

Table 3: Constraint active search is able to produce many more satisfactory outcomes for consideration in eventual fabrication. It does this, in part, by being able to more quickly terminate unsatisfactory outcomes through use of the Gaussian process model.

Figure 7 provides two sets of plots: the parallel axes graphs which show that for nearly all satisfactory outcomes the Diameter Top should be quite small; and the scatter plots, which show how the other parameters define the satisfactory region. Of greatest note for eventual fabrication, satisfactory cones seems to be of the shorter, fatter variety, with Height consistently less than Diameter Bottom. The best results also seems to prefer some space between cones, with Box Size greater than Diameter Bottom as opposed to roughly equal to Diameter Bottom (as helped minimize reflection in (Haghanifar et al. 2020)). Cone Angle is an auxiliary shape description, provided here to show that there is a specific range of Cone Angle values which is required to see satis-

factory efficiency (within [0.7, 1.0] radians).

Conclusion

We have adapted Constraint Active Search to incorporate estimates of uncertainty generated by the iterative approximation of the emission in each dimension. In doing so, we were able to improve our computational efficiency while still identify a diverse set of satisfactory manufacturing designs.

In future work, we hope to conduct 3D simulations which lead to actual fabrications; doing so may require some multifidelity computations involving lower quality computational grids or more cheaply simulated approximations to the infinite domain. There is also an opportunity to intelligently consider individual dipoles for the x, y and z-axes, rather than computing the same one for each at each step – doing so would allow the axis of most importance to the satisfactory outcome (more than 70% efficiency) to be sampled with the dipoles that provide the most information (through, e.g., Bayesian quadrature (Rasmussen and Ghahramani 2003)) rather than through the QMC strategy.

We also plan to compare the performance of CAS to Bayesian optimization to understand how the iterative approximation strategy performs in that setting. We should also rerun these experiments multiple times to produce some sense of statistical certainty regarding the results.

References

Adachi, C.; Baldo, M. A.; Thompson, M. E.; and Forrest, S. R. 2001. Nearly 100% internal phosphorescence efficiency in an organic light-emitting device. *Journal of Applied Physics*, 90(10): 5048–5051.

Caruana, R.; Lawrence, S.; and Giles, L. 2001. Overfitting in neural nets: Backpropagation, conjugate gradient, and early stopping. *Advances in neural information processing systems*, 402–408.

Choi, S.-C. T.; Hickernell, F. J.; McCourt, M.; and Sorokin, A. 2020+. QMCPy: A quasi-Monte Carlo Python Library.

Fasshauer, G. E.; and McCourt, M. J. 2015. *Kernel-based approximation methods using Matlab*, volume 19. World Scientific Publishing Company.

Glowacki, I.; Jung, J.; Ulanski, J.; and Rybak, A. 2012. 2.33 - Conductivity Measurements. In Matyjaszewski, K.; and Möller, M., eds., *Polymer Science: A Comprehensive Reference*, 847–877. Amsterdam: Elsevier. ISBN 978-0-08-087862-1.

Haghanifar, S.; Gao, T.; Vecchis, R. T. R. D.; Pafchek, B.; Jacobs, T. D. B.; and Leu, P. W. 2017. Ultrahigh-transparency, ultrahigh-haze nanograss glass with fluid-induced switchable haze. *Optica*, 4(12): 1522–1525.

Haghanifar, S.; McCourt, M.; Cheng, B.; Wuenschell, J.; Ohodnicki, P.; and Leu, P. W. 2020. Discovering high-performance broadband and broad angle antireflection surfaces by machine learning. *Optica*, 7(7): 784–789.

Ho, Y.-H.; Chen, K.-Y.; Peng, K.-Y.; Tsai, M.-C.; Tian, W.-C.; and Wei, P.-K. 2013. Enhanced light out-coupling of organic light-emitting diode using metallic nanomesh electrodes and microlens array. *Optics Express*, 21(7): 8535.

Lee, J.-H.; Ho, Y.-H.; Chen, K.-Y.; Lin, H.-Y.; Fang, J.-H.; Hsu, S.-C.; Lin, J.-R.; and Wei, M.-K. 2008. Efficiency improvement and image quality of organic light-emitting display by attaching cylindrical microlens arrays. *Optics Express*, 16(26): 21184.

Lumerical Inc. 2021a. Finite Difference Time Domain (FDTD) solver introduction. https://support.lumerical.com/hc/en-us/articles/360034914633-Finite-Difference-Time-Domain-FDTD-solver-introduction. Accessed: 2021-11-19.

Lumerical Inc. 2021b. Understanding coherence in FDTD simulations. https://support.lumerical.com/hc/en-us/articles/360034902293-Understanding-coherence-in-FDTD-simulations. Accessed: 2021-11-19.

Malkomes, G.; Cheng, B.; Lee, E. H.; and McCourt, M. 2021. Beyond the Pareto Efficient Frontier: Constraint Active Search for Multiobjective Experimental Design. In *International Conference on Machine Learning*, 7423–7434. PMLR.

McCourt, M.; Dewancker, I.; and Ganci, S. 2016. Preemptive Termination of Suggestions during Sequential Kriging Optimization of a Brain Activity Reconstruction Simulation. *arXiv preprint arXiv:1612.04451*.

Pattison, M.; Hansen, M.; Bardsley, N.; Elliott, C.; Lee, K.; Pattison, L.; and Tsao, J. 2020. 2019 Lighting R&D Opportunities. Technical report, Solid State Lighting Solutions (SSLS) Inc., Santa Barbara, CA (United States).

Rasmussen, C. E.; and Ghahramani, Z. 2003. Bayesian monte carlo. *Advances in neural information processing systems*, 505–512.

Schwab, T.; Fuchs, C.; Scholz, R.; Zakhidov, A.; Leo, K.; and Gather, M. C. 2014. Coherent mode coupling in highly efficient top-emitting OLEDs on periodically corrugated substrates. *Optics Express*, 22(7): 7524.

Wei, M.-K.; and Su, I.-L. 2004. Method to evaluate the enhancement of luminance efficiency in planar OLED light emitting devices for microlens array. *Optics Express*, 12(23): 5777.

Williams, E.; Haavisto, K.; Li, J.; and Jabbour, G. 2007. Excimer-Based White Phosphorescent Organic Light-Emitting Diodes with Nearly 100 % Internal Quantum Efficiency. *Advanced Materials*, 19(2): 197–202.

Xiao, L.; Su, S.-J.; Agata, Y.; Lan, H.; and Kido, J. 2009. Nearly 100% Internal Quantum Efficiency in an Organic Blue-Light Electrophosphorescent Device Using a Weak Electron Transporting Material with a Wide Energy Gap. *Advanced Materials*, 21(12): 1271–1274.

Zhang, Q.; Tsang, D.; Kuwabara, H.; Hatae, Y.; Li, B.; Takahashi, T.; Lee, S. Y.; Yasuda, T.; and Adachi, C. 2015. Nearly 100% Internal Quantum Efficiency in Undoped Electroluminescent Devices Employing Pure Organic Emitters. *Advanced Materials*, 27(12): 2096–2100.